Investigations on optical and dielectric properties of PVDF/PMMA blend doped with mixed samarium and nickel chlorides

M. Abdelaziz

Abstract Samarium and nickel ions, singly and in combination, were doped into poly(vinylidene fluoride) (PVDF)/poly(methyl methacrylate) (PMMA) blend. Films were prepared by casting technique. The microstructure of the prepared films were studied using X-ray diffraction (XRD), Infrared (FT-IR) and Fluorescence spectroscopy. The complex formation between Sm^{3+} and/or Ni^{2+} ions with the polymeric chain was confirmed by XRD and FT-IR. XRD analysis revealed that the crystallinity of blend improved by doping. The presence of the dopants led to some changes in the vibrational spectrum of the blend. The effect of doping levels on the optical and dielectric properties of PVDF/PMMA blend was investigated. It was observed that the optical band gap E_g, dielectric constant ε', AC conductivity σ_{Ac} and loss tangent $\tan\delta$ increase significantly with increasing Sm^{3+} content. The correlation between optical and dielectric properties and the microstructure of polymeric systems was studied.

1 Introduction

The contribution of new materials, involving composites and blends, has been reaching the most varied fields of science, as much of the scientific as technological point of view. Poly(vinylidene fluoride) (PVDF), as a semi-crystalline polymer, has wide applications due to its excellent properties such as good mechanical strength, stability against vigorous chemicals, and good thermal stability [1]. Also, PVDF has been widely studied because of its relatively good piezo-electric and pyro-electric response and the influence of its polymorphic forms used in the development of electronic devices [2]. PVDF is widely used in transducers, piezo-electric sensor and infrared imaging and other military and biomedical fields. Compared with the traditional materials, PVDF has good electrical properties and good flexibility, can be easily prepared in low temperature [3].

As PVDF is highly miscible with polymers containing oxygen, which is related to the interaction between the fluorine atoms and carbonyl groups of the partner, several pairs of blends have investigated, such as PVDF/poly(vinyl pyrrolidone) (PVP) [4], PVDF/poly(vinyl acetate) (PVAc) [5] and PVDF/PMMA [6]. Among these polymers, PMMA is more interesting due to its good compatibility with PVDF all over the concentration range in the blend polymer. Kim et al. [7] and Zhang and his works [8] reported that the crystallization behavior of PVDF/PMMA blend was highly dependent on the composition of PMMA in the blend, they observed that the β-phase of PVDF was obtained as the PVDF weight fraction with above 30 wt% and addition of 10 wt% PMMA could favor the growth of β-phase of PVDF crystals.

Rare earth compounds have a significant place among the technologically important materials. They have their importance for the luminescent, photoconductive, photorefractive, laser action, electric, magnetic and superconducting properties. Among the rare earth ions Sm^{3+} ions have stimulated extensive interests due to their potential application for high-density optical memory devices. The excited $^4G_{5/2}$ level of sm^{3+} ions emits in the visible region which exhibits relatively high quantum efficiency and shows different quenching mechanisms which make sm^{3+}

M. Abdelaziz (✉)
Natural Science Department, RCC, King Saud University, Riyadh, Kingdom of Saudi Arabia
e-mail: mabdelaziz62@yahoo.com

M. Abdelaziz
Physics Department, Faculty of Science, Mansoura University, Mansoura 35516, Egypt

ions an interesting case to analyze the energy transfer process [9]. Polymeric films doped with lanthanide ions have received extensive attention because of their potential application as optical switches for visible and near infrared radiation, optical detectors, laser and sensors [10].

several studies have been reported on PVDF/PMMA blend [6, 10], but it seems that there are no investigations on influence of doping with Sm^{3+} and/or Ni^{2+} mixed dopants on the microstructure, optical and dielectric properties of PVDF/PMMA blend. The present work constitutes a preliminary study within a broader project of our group that intends to follow and understand the changes at the micro-structural level of composites materials. This investigation aims to produce composites with new properties such as high dielectric constant, high AC conductivity, and enhancement of piezo- and pyro-electric coefficients of PVDF using a series of complementary techniques, including FT-IR, XRD, fluorescence spectroscopy and optical and dielectric properties.

2 Materials and experimental methods

2.1 Materials and films preparation

Poly(vinylidene fluoride) pellets (SOLEF 1008, Solvay, Belgium) with average molecular weight 5.3×10^5 and PMMA in the powder (BDH chemical Ltd., UK.) with average molecular weight of 1.2×10^5 were used. Firstly, both PVDF and PMMA were dissolved in DMF, separately. The polymer blend of PVDF and PMMA with mass ratio of 90/10 was prepared via a solution mixing and casting technique. Different concentrations of $SmCl_3$ and $NiCl_2$ according to relation $xSmCl_3$ $(15 - x)$ $NiCl_2$, where x = 0, 3, 5, 7.5, 10, 12, and 15 wt%, were dissolved in DMF. The request solution of $SmCl_3$ and $NiCl_2$ were added to the blend solution at a suitable viscosity. The mixtures of the dissolved polymers with the dopants were stirred on magnetic stirrer and then cast onto a glass dish and kept in a dry atmosphere at 323 K for 2 weeks to minimize the solvent traces. PVDF/PMMA (90:10) films with different mass fractions (x) were prepared. The thickness of films was in the range of 100–150 μm. The doping level x (wt%) was calculated from the following equation

$$x(\text{wt\%}) = \frac{x_d}{x_p + x_d} \times 100 \tag{1}$$

where x_p and x_d represent the weight of polymer and dopant respectively.

2.2 Analytical methods

X-ray diffraction of the samples was carried out using a Siemens Type F diffractometer with Cu K_α radiation and a

LiF mono chromator. An infrared spectrophotometer (Perkin Elmer 883) was used for measuring the IR spectra in the wave number range 400–4,000 cm^{-1}. Ultra violet and visible absorption spectra were measured in the wavelength range 200–900 nm using a Perkin Elmer UV/VIS spectrometer. The fluorescence emission spectra of pure PVDF/PMMA blend and blends doped with different Sm^{3+}/Ni^{2+} ratio were recorded at room temperature using FluroMax- 2 spectroflourophotometer. The wavelength accuracy of emission was ± 1 nm. The dielectric constant (ε'), dielectric loss (ε''), AC conductivity (σ_{AC}) and relaxation time (τ) of the undoped blend and doped blend are determined by measuring capacitance C and loss tangent (tanδ) using an AC impedance bridge (WAYNE KERR precision component analyzer model 6440B) at room temperature in frequency ranging of 20–3 MHz. The dielectric constant (ε') is evaluated from the capacitance measurements using the following equation.

$$\varepsilon' = \frac{C}{C_o} \text{ and } c_o = \varepsilon_o \frac{A}{d} \tag{2}$$

where C_o is the vacuum capacitance of any configuration of electrodes and C is the capacitance with isotropic material filling the space. A is the cross section area of the sample and d is the thickness.

Relaxation times of the complexes are obtained from the study of tanδ as a function of frequency. For maximum dielectric loss, the absorption peak is described by the relation $\tau\omega \approx 1$, where τ is the relaxation time and ω is the angular frequency of the applied signal.

3 Results and discussion

3.1 X-ray diffraction (XRD)

Figure 1 displays the XRD scans of PVDF, PVDF/PMMA blend, and its composites with different ratio of dopants. The spectrum of pure PVDF shows some diffraction peaks at $2\theta = 18.51^o$, 20.09^o, 25.8^o and 38.87^o, indicating main crystalline phases α, β and γ of PVDF [11]. The assignment of these crystalline peaks is listed in Table 1. When PMMA is added to PVDF, the peak intensity of β-phase is higher and becomes sharper than that in pure PVDF, indicating that the addition of small amount of PMMA can promote the molecules in PVDF to more regular, then resulting in increased crystallinity of PVDF. This suggests that the PMMA is able to interact with PVDF chains in the amorphous regions and at inter-phases to prohibit PVDF segments diffusion towards the crystallization fronts. This causes a kind of stretching at molecular level which results in the end-to-end orientation of PVDF chains and produces all-trans conformations which chiefly crystallize to β crystal.
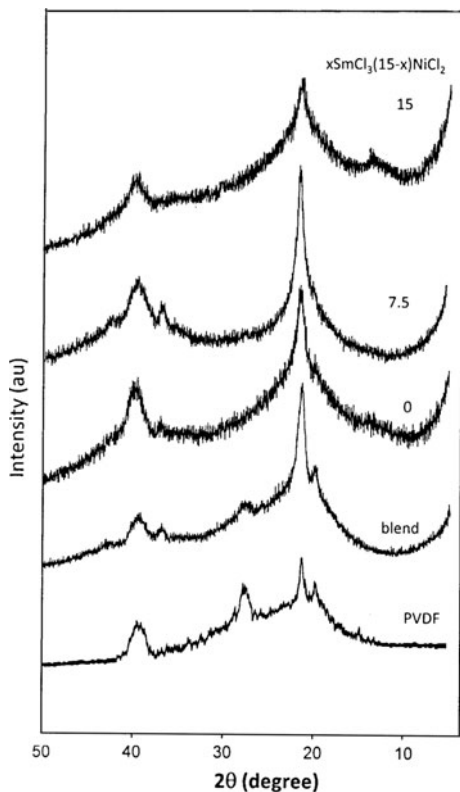
Fig. 1 XRD patterns of pure PVDF, blend and blend doped with Sm^{3+} and/or Ni^{2+} ions

Table 1 X-ray diffraction peaks and their assignments of the prepared films

Sample	2θ	Assignments
PVDF	18.51°	(110) α
	20.09°	(110) β, (200)β
	25.8°	(021) γ
	38.87°	(002) α
PVDF/PMMA	18.51°	(110) α
	20.09°	(110) β, (200)β
	25.8°	(021) γ
	36.27°	(001) β
	38.87°	(002) α
x = 0	20.09°	(110) β, (200)β
	36.27°	(001) β
	38.87°	(002) α
x = 7.5	20.09°	(110) β, (200)β
	38.87°	(002) α
x = 15	14.5°	–
	20.09°	(110) β, (200)β
	38.87°	(002) α

When Sm^{3+} and/or Ni^{2+} are present as dopants in the blend, the XRD patterns show intense peaks at about $2\theta = 18.5°$, 20.09°, 25.8°, 36.27° and 38.87°. From the

spectrum at doping level x = 0 wt%, the intensity of both diffraction peaks at $2\theta = 20.09°$ (β-phase) and 38.87° (α-phase) of the composites increases. This increase arises from crystallite of Ni [12]. Also, the XRD diffraction peaks at $2\theta = 18.51°$, 25.8° and 26.27° disappeared. For increasing doping levels x > 0 wt%, increasing samarium content and decreasing nickel content in the blend, the intensity of these diffraction peaks increases up to x = 7.5 wt% and then decreases and becomes broadened and tends towards the amorphization due to increase in un-saturation and free radicals, which led to destruct the molecular regularity of PVDF. Moreover, when the blend is doped with doping level x = 15 wt%, there is a new diffraction peak at $2\theta = 14.5°$ was observed, indicating a complex formation between the dopants and polymeric matrix.

According to the area under the peaks of β-phase and α-phase, the dependence of the values of the ratio on doping levels is listed in Table 2. As shown in Table 2, the relative content of β-phase increased with the increase in doping levels up to x = 7.5 wt%, indicating that the increase in samarium content promotes the formation of β-phase. However, when the doping level increased more than 7.5 wt%, characteristic peaks of PVDF decreased, which means that the crystallinity of PVDF decreased a lot. This is due to the fact that too much $SmCl_3$ in PVDF/ PMMA blend destruct the molecular regularity of PVDF. Similar behavior has been observed by Qi et al. [13].

3.2 FT-IR spectroscopy

FT-IR spectroscopy is important in the investigation of polymer structure that provides information about the complexation and interactions between the various constituents in the polymeric matrix. FT-IR spectra of pure PVDF, PVDF/PMMA blend and doped blends are shown in Fig. 2. Main characteristic vibration peaks of PVDF are observed in Fig. 2 and their assignments are given in Table 3 [14]. As evident in Fig. 2, the indentified peaks at

Table 2 Dependence of relative area under β–phase to α–phase A_β/A_α, fraction of β-phase content F(β), the refractive index),dielectric loss ε'' on doped levels

x (wt%)	A_β/A_α	n	F(β) %	ε''
0	1.55	2.015	53.65	0.114
3	–	2.209	72.53	0.0931
5	–	2.51	78.50	0.124
7.5	3.8	2.617	83.12	0.093
10	–	2.23	77.6	1.821
12	–	2.17	66.6	2.072
15	2.85	2.038	62.2	2.595

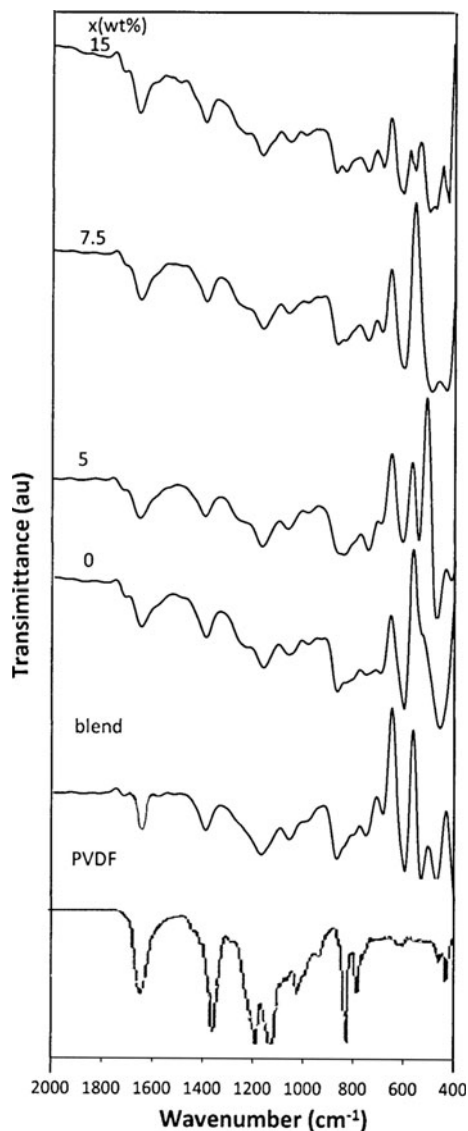**Fig. 2** FT-IR spectra of pure PVDF, PVDF/PMMA blend and (blend doped with different Sm^{3+}/Ni^{2+} ratio)

890, 1,120 and 1,186 cm^{-1} are absent in the spectrum of PVDF/PMMA blend. New vibration peaks at 543, 702 assigned to presence of head-to-head and tail-to-tail configuration, and 797 cm^{-1} are observed. The new absorption bands may be correlated likewise to defects induced by the charge transfer reaction between the polymer chain and the dopant [15]. This result was confirmed with that obtained from XRD. After the addition of samarium and/or nickel ions, the observed peaks at 460 and 835 cm^{-1} are shifted to higher frequencies. Also, the intensity of these vibrations notably decreased upon doping levels. The presence of the dopants leads to some changes in the vibrational spectra of the doped samples, which confirms that there is a strong interaction between Sm^{3+} and Ni^{2+} ions and the host matrix which leads to the formation of the polymer complex.

For prepared films containing α -phase and β–phase, the relative fraction of β–phase, F(β), present in each samples can be calculated using the following relation [16]:

$$F(\beta) = \frac{X_\beta}{X_\beta + X_\alpha} = \frac{A_\beta}{1.26A_\alpha + A_\beta} \tag{3}$$

where X_α and X_β refer to crystalline mass fractions of α-phase and β-phase, respectively. A_α and A_β correspond to the height of absorption bands for α-phase (610 cm^{-1}) and β-phases (830 cm^{-1}). The variation of relative β-phase content against the doping levels is demonstrated in Table 2. It is clearly obvious that β-phase content increases markedly and then decreases indicating a maximum value of β-phase content at doping level x = 7.5 wt%. The FT-IR technique was successfully used to quantify the variations of β-phase, and these results were confirmed by XRD analysis.

3.3 Fluorescence spectra

Fluorescence is a sensitive technique with the fluorescence properties of a molecule and its local environment. Generally, fluorescence can be sensitive to variations of polarity, dielectric constant, viscosity and PH. Examination of the fluorescence spectra of PVDF/PMMA blend and its composites is shown in Fig. 3. The polymeric films were excited at the wavelength of 380 nm. It is observed that the spectrum of the blend exhibits a broad maximum fluorescence peak at about 550 nm indicating a specific medium effect such as hydrogen bonding, physical rotation of the polar group (CH_2–CF_2) of PVDF or some other interactions [17]. The dependence of the fluorescence intensity of the maximum fluorescence peak on doping levels is observed in Fig. 4. It is well known that the maximum value of the fluorescence peak is shown at equal weight fraction from samarium and nickel indicating that the polarity of the medium gradually increases. The strong increase in the fluorescence anisotropy is due to the higher content of β-phase of this sample. The observed trend is related to dipolar interaction between the dopants and the host polymer. This result is in agreement to that obtained from XRD and FT-IR.

Moreover, the spectrum of the blend doped with samarium only shows two fluorescence peaks at 600 and 647 nm corresponding to spin allowed transitions $^4G_{5/2} \rightarrow {}^6H_{7/2}$ and $^4G_{5/2} \rightarrow {}^6H_{9/2}$ respectively, which is characteristic to an octahedral geometry of Sm^{3+} ions [18].

3.4 Optical absorption

3.4.1 Spectrum characterization

The UV–Vis absorption spectra of undoped blend and blend containing samarium and nickel ions, singly and in combination,

Table 3 Characteristic bands with specific vibrational modes and related to crystalline phases of PVDF

$\nu(cm^{-1})$	Group	Vibration	Comments
460	CF_2	Bending and wagging	β-phase
610	CF_2	Bending	α-phase
780	CH_2	Rocking	α-phase
830	CH_2	Rocking	γ andβ-phase
890	CF_2	Stretching	β -phase
1,020	CH2	Wagging	γ-phase
1,110	C–C–C	Bending	–
1,180	C–O	Stretching	–
1,340	CH_2	Out-of phase bending (wagging or twisting)	γ-phase
1,640		Trans-disubstituted ethylene	DMF solvent
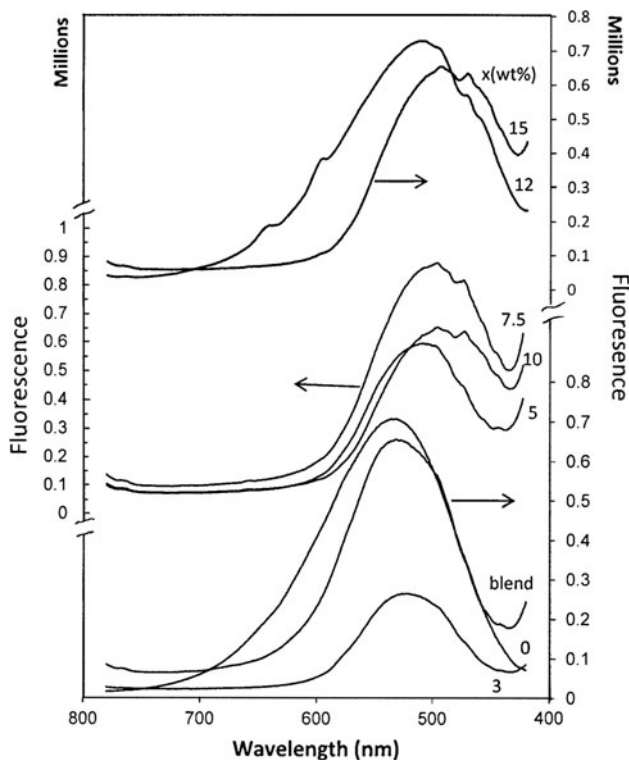
Fig. 3 Fluorescence spectra of blend and its composites

Fig. 4 The dependence of fluorescence intensity and peak position on doping level

are shown in Fig. 5. The undoped sample shows shoulder like band nearly at 280 nm due to the carbonyl groups associated with ethylene un-saturation which indicates the presence of conjugated polyene double band [19]. Upon addition of 15 wt% $NiCl_2$ to the blend, the spectra exhibit the two characteristic bands at 650 and 670 nm corresponding to spin allowed transitions $^3A_{29}$ (F) → $^3T_{19}$ (F) and $^3A_{29}$ (F) → $^3T_{19}$ (p) respectively, which is characteristic to an octahedral geometry of Ni^{2+} [20]. When both Sm^{3+} and Ni^{2+} ions are present as dopant, the spectra show a shift in the absorption edge towards higher wavelength indicating the decrease in the optical band gap. Also the decrease in the absorbance of the two absorption peaks of Ni^{2+} is observed. For the doping
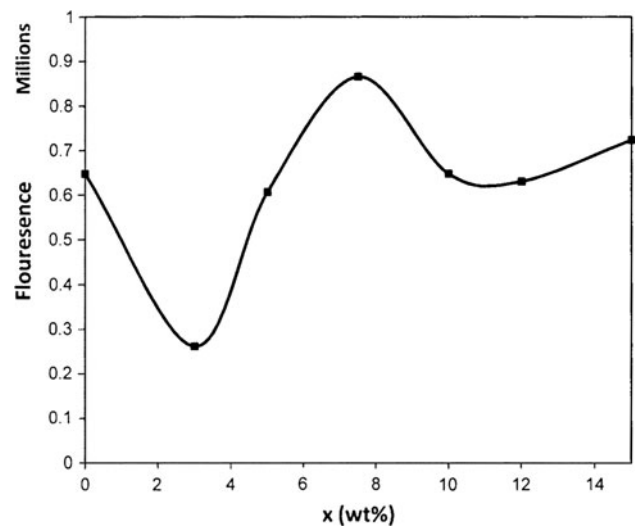
level x ≥ 5 wt%, the spectra show characterizing absorption band at 380 nm. The absorption bands of Sm^{3+} are classified into two groups; the first one is the lower energy group which lies between 900 and 1,800 nm, not shown here, and the second one is higher energy group, which lies between 350 and 600 nm. The majority of the transitions in the spectra originate from induced electric dipole interactions. In the visible region, all the transitions are spin forbidden and hence the absorption bands are weak in intensity. So the transition at 380 nm is assigned f → f transitions from the ground $^6H_{5/2}$ state to various excited states of sm^{3+} ions [9].

3.4.2 Optical energy band gap (E_g) and refractive index (n)

The optical absorption spectrum is an important tool to obtain optical energy band gap of crystalline and amorphous materials. In order to determine optical energy band gap of the films, the absorption coefficient was determined from the spectra using the formula.
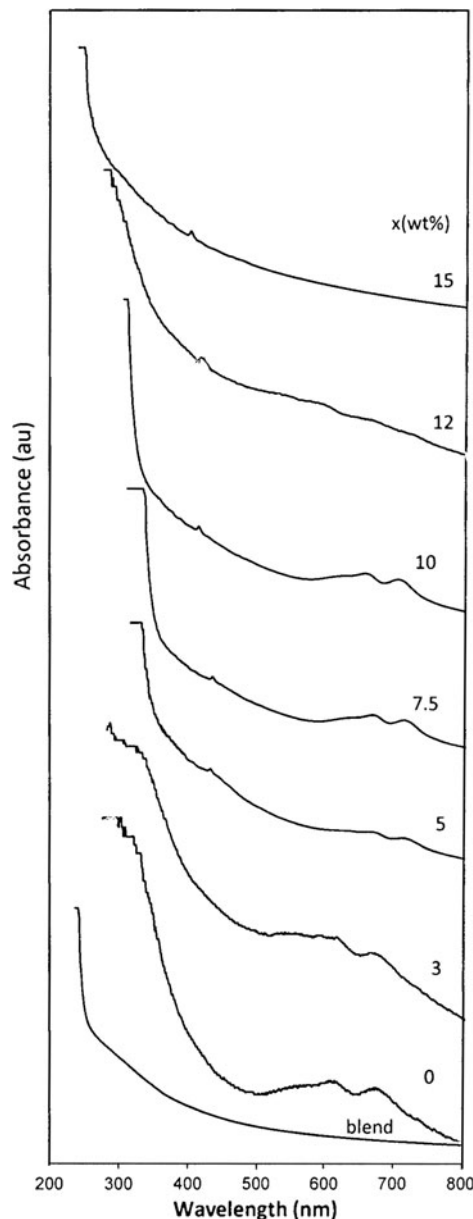
Fig. 5 Absorption spectra of PVDF/PMMA and blend doped with various concentrations

$$\alpha = \frac{\ln \frac{1}{T}}{d} \tag{4}$$

where T is the transmittance and d is the film thickness. The optical energy band gap of the films was determined from the absorption spectra near the absorption edge. The absorption coefficient can be related to the energy of the incident photon hν according to Mott and Davis formula [21].

$$\alpha(v) = B \frac{(hv - E_g)^r}{hv} \tag{5}$$

where B is a constant, hν is the photon energy and E_g is the optical band gap, r is an exponent which can take values of 1, 2, 3, 1/2, 3/2 depending on the nature of the electronic transitions responsible for the optical absorption. The best value of (r) can be determined from the slope of the linear part of $(\alpha h\nu)^{1/r}$ versus hν. The best straight line may be obtained when r = 1/2 for all examined films. This suggests that the transition energy for electrons may account for indirect allowed transition. So the indirect optical energy band gap (E_g) was evaluated from $(\alpha h\nu)^2$ versus hν plots from the linear parts of these curves as shown in Fig. 6. The variation of optical energy band gap (E_g) values vs doping levels is shown in Fig. 7. It is clear that the optical band gap decreases up to doping level x = 7.5 wt% and then increases when increasing the doping level up to x = 15 wt%. The decrease in E_g may be explained by invoking the occurrence of local cross linking within the amorphous phase of the polymer, in such a way to increase the degree of ordering in these parts [22]. Another reason could be that the drop of E_g may be due to the variation of non-bridging oxygen (NBO). The NBO bonds have a much greater ionic character and much lower bond energy. Consequently, the NBO bonds have higher polarizability leading to decrease in Eg. The increase in E_g, for doping level x > 7.5 wt%, may be due to increasing the localized defect in the polymeric matrix.

Refractive index (n) of the composite was calculated by using the relation [22].

$$\frac{n^2 - 1}{n^2 + 2} = 1 - \sqrt{\frac{E_g}{20}} \tag{6}$$

The dependence of the refractive index on doping level is listed in Table 2. As per Table 1 that the refractive index shows a maximum at doping level x = 7.5 wt%. The refractive index depends on the polarizability of the material. The more polarizable the outer electrons tend to the higher refractive index.

3.5 Dielectric studies

The dielectric behavior of undoped blend and its complexes were studied and the results are analyzed in terms of different parameters. It was noticed that the phase angle was always negative, indicating that the complexes were capacitive and could be represented by parallel RC networks connected in series.

3.5.1 Dielectric behavior (ε′)

The complex permittivity (ε*) or dielectric constant of a system is defined by

$$\varepsilon* = \varepsilon\prime - j\varepsilon\prime\prime \tag{7}$$
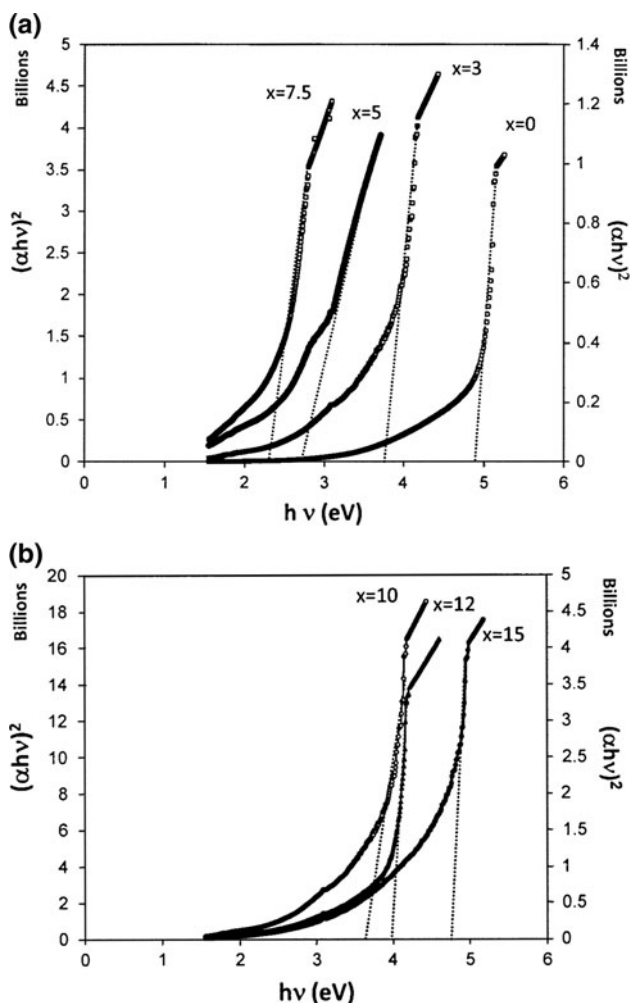
Fig. 6 The dependence of $(\alpha h\nu)^2$ on photon energy (hν), **a** 1
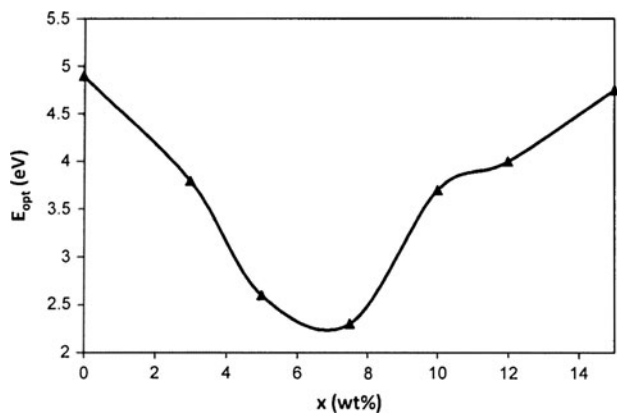
Fig. 7 The dependence of the optical band gap E_g on the doping levels

Fig. 8 Variation of dielectric constant ε' as a function of frequency. Figure 8 (*inset*) the dependence of dielectric constant ε' on doping levels at certain frequency 10 kHz

where ε' is the real part of dielectric constant, ε'' the imaginary part of dielectric constant of the material. Figure 8 shows the variation of dielectric constant ε' of all samples a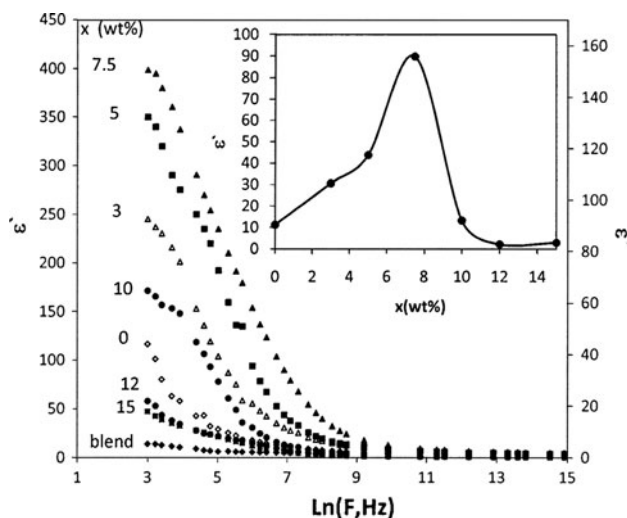s a function of frequency at room temperature. In all cases, a strong frequency dispersion of permittivity is observed in the low frequency region followed by a nearly frequency independent behavior above 10 kHz. The higher values of ε' at lower frequency were due to the simultaneous presence of space charge, dipolar, ionic and electronic polarizations. The polarization was obtained by the space- charge polarization and led to hopping exchange of charge carriers between the localized states and resultant displacement of dipoles with respect to the applied field [23].

The dependence of the dielectric constant (ε') on the doping levels is shown inset Fig. 8. It is observed that the dielectric constant shows a maximum value at equal fraction of samarium and nickel. The variation of the dielectric constant was discussed based on the x-ray studies which confirmed that PVDF is present as mixed α, β and γ phases. The increase in the dielectric constant with substitution of Sm^{3+}/Ni^{2+} ratio is due to the increase in the polar β-phases in the samples, which increases the different polarization mechanisms. On the other hand, the increase in dielectric constant when increasing samarium content may be due to the various polarization mechanisms. The 4f-4f hybridization increases the valence exchange in the Sm^{3+}-doped samples and contributes to the polarization [24]. While the decrease in the dielectric constant after doping level $x = 7.5$ wt% is due to the increase in non polar α-phase and decrease in the polar β-phases in the sample. Due to the nonpolar nature of PVDF, the constrained polymer chain is hindering the formation of electrical polarization.

Figure 9 shows the frequency dependence of ε'' for all samples. Only a single broad peak in the dispersion relation was observed. It was clear that the values of ε''_{max} (f) were higher for doped blend than undoped blend. The increase in
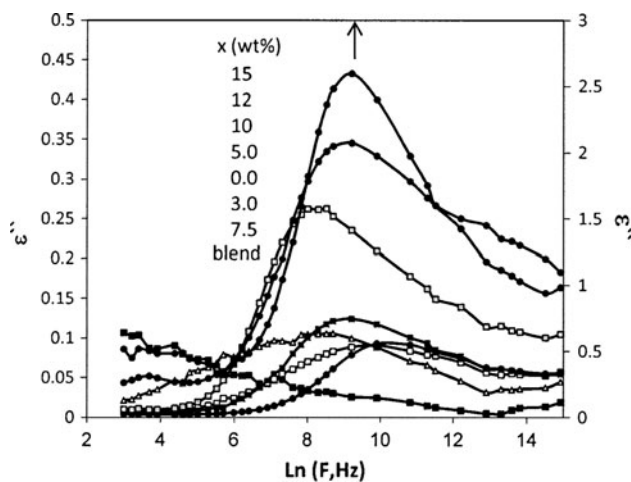
Fig. 9 Variation of dielectric loss ε'' with frequency

Fig. 10 Variation of AC conductivity σ_{AC} with frequency. Figure 10 (*inset*) the dependence of AC conductivity σ_{AC} on doping levels at certain frequency 10 kHz

ε'' could be ascribed to α and β relaxation process in which the side groups cooperated with the backbone motion in a micro-Brownian motion. Also, the polar nature of the molecules increased the polarization process and caused the shift of the dipole segmental and dipole group relaxation to higher frequencies. The dependence of dielectric loss on doping levels is listed in Table 2. It is clear that the minimum value of dielectric loss is observed at doping level x = 7.5 wt%. The minimum value of dielectric loss is due to inhibition of domain-wall motion.

3.5.2 AC conductivity

The AC conductivity (σ_{AC}) of the samples was calculated using the dielectric equation [25].

$$\sigma_{AC} = 2\pi f \varepsilon_0 \varepsilon_r \tan \delta \qquad (8)$$

where f is the frequency of the applied field, ε_0 is the permittivity of free space and $\tan\delta$ denotes the dielectric loss tangent. Figure 10 shows the variation of AC conductivity as a function of frequency for undoped and doped blends at room temperature. It was observed that, in all samples, AC conductivity was constant up to 10 kHz and thereafter increased steeply. The higher conductivity at higher frequencies confirmed the short range intra-well hopping of charge carriers between localized states. The dependence of the AC conductivity on the doping level is shown inside Fig. 10. It can also be seen that the AC conductivity increases with the increase in doping levels up to 7.5 wt% and then decreases. The increase in AC conductivity may be attributed to the fact that the dopants of Sm^{3+} and Ni^{2+} are acceptors for polymeric matrix and are usually compensated by the formation of oxygen vacancies. Thus, the increase in dopant concentration form Sm^{3+} increases the oxygen vacancies which results in an increase in free electron density and conductivity. The decrease in
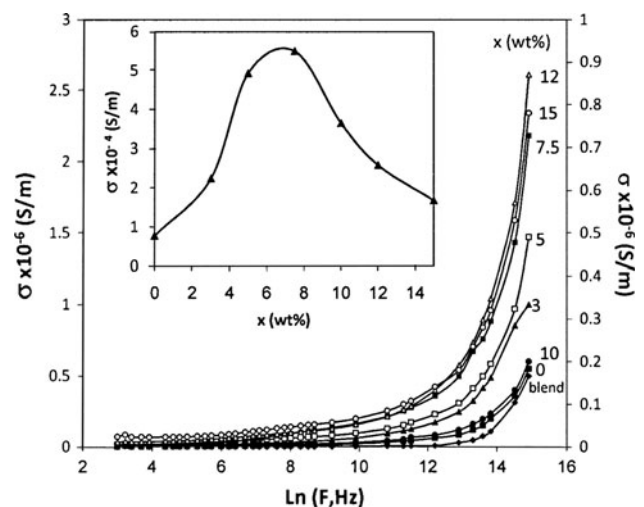
AC conductivity arises from the decrease of the effective number of charge carriers involved in doping mechanism.

3.5.3 The dissipation factor tan δ

Dielectric loss is usually used to characterize the motivation of different dipole moments under different electric fields and frequencies. Figure 11 shows the frequency response of the loss tangent tanδ achieved at room temperature for all samples. The exponential demise of tangent losses tanδ can be marked as a function of frequency for blend and blend doped with doping level x = 0 wt%. These types of variations in the dielectric losses are considered to be caused by domain wall resonance. In other words, the higher dielectric loss tangent at a low frequency is due to PVDF crystals. Similar behavior of loss tangent is reported by Z. Zhang [26]. Also, it can be found that the tanδ of doped blends is higher when compared to the undoped blend. It is well known that the dielectric loss depends on the conducting natural of material, the incorporation of dopants into blend increases its conductivity, which seems to increase the dielectric loss of the doped blend as compared to undoped blend. As shown in Fig. 12, the variation of loss tangent tanδ with frequency for blend doped with x > 0, the loss tangent spectra were characterized by peaks appearing at lower frequencies suggesting the existence of relaxing dipoles in all the samples. The peak shifts to higher frequency with the increase in dopant concentrations. The graph also shows that the height of the peak increases with the dopant concentration as relaxation time increase. As we know, two molecular motions, the micro-Brownian motion of non-crystalline chain segments (β-relaxation) and the molecular motion onto the amorphous/crystalline interfaces
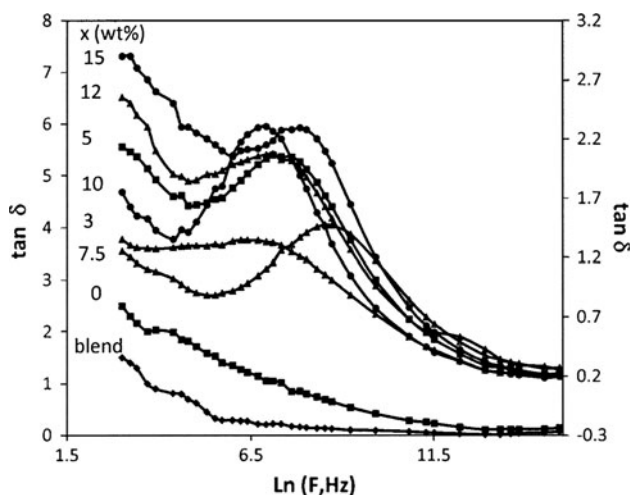
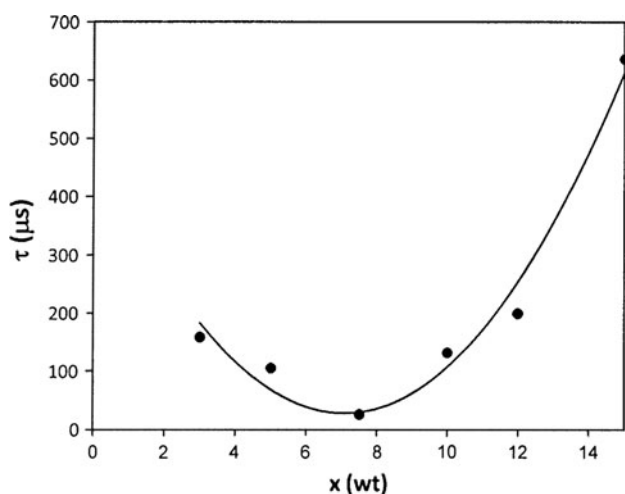**Fig. 11** Variation of dielectric loss tanδ against frequency

Fig. 12 Variation of loss tangent tanδ with the doping levels

have been proposed to be responsible for the relaxation process. The relaxation time, T for the prepared films at different doping levels was obtained from renowned Havriliak Negami relationship [27].

$$\tau = \frac{1}{2\pi f_0} \qquad (9)$$

where f_0 is the relaxation time. Figure 12 shows the relaxation time for the composite films at different concentration of dopants. From the graph, one can conclude that the relaxation time decreases up to doping level x = 7.5 wt% and then increases showing a minimum value with numerical equation.

$$\tau = 9.35\,x^2 - 132.5x + 497.7 \qquad (10)$$

where x is points to doping level. The decrease in relaxation time indicates that multiple path of the system to be

relaxed is due to high availability of free charges. These results confirm the explanation for the dielectric constant and dielectric loss characteristics as relaxation times decrease with the increasing dopant concentration.

4 Concluson

Polymeric films of PVDF/PMMA doped with different ratio of Sm^{3+}/Ni^{2+} ions were prepared by casting technique. Spectroscopic and dielectric investigations were carried out of the prepared films. The complexation of the dopants with the polymer matrix was confirmed by XRD and FTIR studies. Fluorescence spectra of blend doped with Sm^{3+} and/or Ni^{2+} show a strong emission peak at 550 nm beside two weak emission peaks at 600 and 647 nm. The change in the optical absorption spectra is due to complex formation which can be reflected in the form of decrease in optical band gap. It was found that dielectric constant ε', dielectric loss ε'', AC conductivity σ_{AC}, dielectric loss tangent tanδ and relaxation time τ were strongly dependent upon the doping type and doping concentration. The data revealed that the dielectric constant exhibit the normal dielectric behavior and decrease with the increase in frequency. The improvement of dielectric permittivity with the incorporation of Sm^{3+} and/or Ni^{2+} could be originated from the interfacial polarization effect. The conductivity was found to increase with the increase in frequency as well as dopants concentration. The dielectric behavior exhibits a relaxation peak which may be due to the orientation of polar groups present in the polymeric matrix.

The entire observations from present work reveals at x = 7.5 wt% composition has high polar β– phase content, maximum fluorescence, lower optical band gap E_g, higher dielectric permittivity and AC conductivityσ_{AC}, which in turn suggests that this composite is more attractive in various applications, for example, in molecular electronics and embedded capacitor devices.

References

1. S. Rajabzadeh, T. Maruyama, Y. Ohmukai, T. Sotani, H. Matsuyama, Separ. Purif. Technol. **66**, 76–83 (2009)
2. B. Mohammadi, A.A. Yousefi, S.M. Bellah, Polym. Test. **26**, 42–50 (2007)
3. J. Li, Q. Meng, W. Li, Z. Zhang, J. Appl. Polym. Sci. **122**, 1659–1668 (2011)
4. V. Panwar, K. Cha, J. Park, S. Park, Sensor. Actuat. B- chem. **161**, 460–470 (2012)
5. R. Baskaran, S. Selvasekarapandian, N. Kuwata, J. Kawamura, T. Hattori, Mater. Chem. Phys. **98**, 55–61 (2006)
6. A.A. Yousefi, Iranian. Polym. J. **20**, 109–121 (2011)
7. K.J. Kim, Y.J. Cho, Y.H. Kim, Vib. Scpectrosc. **9**, 147–159 (1995)

8. W. Ma, J. Zhang, X. Wang, S. Wang, Appl. Surf. Sci. **253**, 8377–8388 (2007)
9. O. Ravi, C.M. Reddy, L. Manoj, B.D.P. Raju, J. Mol. Struc. **1029**, 53–59 (2012)
10. S. Ray, A.J. Easteal, R.P. Cooney, N.R. Edmonds, Mater. Chem. Phys. **113**, 829–838 (2009)
11. A.E. Abdel Baieth, I.S. Elashmawi, N.H. Hakeem, J. Can, Scient. Indust. Res **3**, 227–237 (2012)
12. S. Kumar, S.K. Chakarvarti, J. Mater. Sci. **39**, 3249–3251 (2004)
13. Y. Qi, L. Pan, L. Ma, P. Liao, J. Ge, D. Zhang, Q. Zheng, B. Yu, Y. Tang, D. Sun, J. Mater. Sci: Mater. Electron (2012). doi:10.1007/s10854-012-0948-6
14. S.L. Mendez, J.F. Mano, A.M. Costa, V.H. Schmidt, J. Macromol. Sci. Phys. B **40**, 517–527 (2001)
15. M.E. Nicho, H. Hu, Solar Energ. Mater. Solar Cells **63**, 423–435 (2000)
16. C.W. Tang, B. Li, L. Sun, B. Lively, W.H. Zhong, Euro. Polym. J. **48**, 1062–1072 (2012)
17. P. Martins, J.S. Nunes, G. Hungerford, D. Miranda, A. Ferreira, V. Sencadas, S.L. Mendez, Phys. Lett. A **373**, 177–180 (2009)
18. C.E. Malashkevich, V.N. Sigaev, N.V. Golubev, EKh Mamadzhanova, A.A. Sukhodola, A. Paleari, P.D. Sarkisov, A.N. Shimko, Mater. Chem. Phys. **137**, 48–54 (2012)
19. M. Abdelaziz, J. Appl. Polym. Sci. **108**, 1013–1020 (2008)
20. S. Chandra, A. Kumar, Spectrochim. Acta: A **68**, 1410–1415 (2007)
21. E.A. Davis, N.F. Mott, Philos. Mag. **22**, 903 (1970)
22. B. Eralah, Bull. Mater. Sci. **29**, 375–378 (2006)
23. A.K. Zak, W.C. Gan, W.H. AbdelMajid, M. Darroudi, T.S. Velayutham, Ceram. Int. **37**, 1653–1660 (2011)
24. A.K.A. Gafoor, J. Thomas, M.M. Musthafa, P.P. Pradyumnan, J. Electron Mater. **40**, 2152–2158 (2011)
25. A.K.A. Gafoor, M.M. Musthafa, K.P. kumar, J. Mater. Sci.: Mater. Electro **23**, 2011–2016 (2012)
26. Q. Meng, W. Li, Y. Zheng, Z. Zhang, J. Appl. Polym. Sci. **116**, 2674–2684 (2010)
27. M.H. Harun, E. Saion, A. Kassim, E. Mahmud, M.Y. Hussain, I.S. Mustafa, J. Adv. Sci. Arts **1**, 9–16 (2009)